Publisher: Engineering College, Al Muthanna University

Open Access

DOI:10.52113/3/eng/mjet/2026-14-03-/38-56, Vol. (14), Issue (3), (2026)

Muthanna Journal of Engineering and Technology MJET

Submitted 25 April 2026, Accepted in revised form 02 June 2026, Published online 04 June 2026

Evaluating the Impact of Porosity–Permeability Heterogeneity on Oil Production in Carbonate Reservoirs

Mohammed elan Mohammed*

Al-Doan Government Technical University, Petroleum Engineering, Production Department
**Corresponding author E-mail: moh96elan@gmail.com*

Abstract

Carbonate reservoirs are home to over 60% of the world's conventional hydrocarbons; however, the complexity of carbonate reservoirs at the pore level creates a very weak correlation between porosity and permeability (ϕ-k). Current models do not account for variations in pore types that affect production rates and thus lead to inaccurate placement of oil wells and inaccurate production forecasts. This research presents a new quantitative method to evaluate variations in ϕ-k in relation to production through the integration of core analysis, wellbore data, and dynamic reservoir simulation. Data used in this study has been compiled from three carbonate oil fields, the Middle East, North America, and Europe, with more than 500 core plugs that were obtained between 1970 and 1999, resulting in analyses of helium porosity and Klinkenberg-corrected permeability (of the cores). Additional characterization was performed on these plug samples using thin-section petrography, micro-CT, and mercury injection capillary pressure. Different groups of pore types were identified and then numerical multi-phase modelling simulating gas-to-oil relative permeability conditions (using the CMG IMEX program), as well as two different statistical regression methodologies (including power law and Kozeny-Carman) were conducted using varying degrees of ϕ-k throughout the reservoirs.

Secondary porosity (such as vugs and fractures) often governs the production of hydrocarbons. However, degradation of porosity-permeability predictability arises from more than simply their existence; it is also caused by factors affecting pore connectivity (such as throat size and throat size distribution) and the continuity of the network. The inclusion of empirical coefficients for vug connectivity will improve hydrocarbon production predictions. For carbonate reservoirs with permeability > 10 mD, hydrocarbon production sensitivity to permeable rock mass will be approximately three times greater than that of porous rock mass. (Experimenting showed that vug network connectivity will enhance the modelling of production rate as a result). The current research applies a class of empirical formulations based on different classes of pore type to modify Darcy's equation and makes completion recommendations for reservoir engineers. The resulting multivariate regression (R^2 = 0.81, MAPE = 18%) provides a superior predictive capability over existing models and presents a credible physical model for reservoir engineers to use.

Keywords: *Carbonate reservoirs, porosity–permeability relationship, oil production rate, pore-type classification, carbonate productivity index.*

1. Introduction

1.1 Challenges of Carbonate Reservoirs and the Porosity–Permeability Relationship

In carbonate reservoirs, which contain more than 60% of conventional oil worldwide, there exists a high degree of heterogeneity caused primarily by diagenetic processes (e.g., dolomitization, dissolution, cementation, fractures) that creates

This is an open access article under the terms of the Creative Commons Attribution License, which permits use, distribution and reproduction in any medium, provided the original work is properly cited. © 2025 The Authors

ongoing challenges to correctly predicting production. While siliciclastic reservoirs often have relatively consistent relationships between porosity and permeability (ϕ and k), carbonate reservoirs demonstrate a wide range of these relationships resulting in extreme difficulty in applying Darcy's law to predict production rates (Q). Production rate (Q) is a direct function of effective permeability (k); however, the variability of k in carbonate reservoirs is strikingly different from that of typical clastic reservoirs, with the maximum range being on the order of several orders of magnitude. While the average amount of pore space (porosity) remains essentially constant in most carbonate reservoirs, the amount of flow capacity varies dramatically depending on the particular carbonate rock type. The inconsistency between pore volume and flow capacity further renders unreliable the use of conventional porosity-permeability transformations originally developed for clastic reservoirs. This ultimately results in either under- or over-drilling, poor completion techniques, and large amounts of economic risk.

1.2 Previous Classifications and Their Link to Production

The assessment of carbonate reservoirs has historically relied on the Lucia Classification (Lucia, 1995) which groups carbonates into three categories based on pore type; Class 1 (interparticle porosity), Class 2 (vuggy porosity), and Class 3 (fractured porosity). The Lucia Classification is a well-established and widely used classification scheme, but there are significant limitations to its use when establishing production potential. Jennings and Lucia (2003) found that for many lithotypes of carbonate, R2 (coefficients of determination) between porosity and permeability is less than 0.4; in other words, less than 40 per cent of the variability in permeability can be accounted for by porosity. Therefore, the production potential of carbonate reservoirs will require a more comprehensive investigation of the various factors that influence production rates, rather than dependence solely on the $\phi - k$ relationship.

1.3 Effects of Reservoir and Fluid Properties, and Flow Models

Carbonate rocks have a combination of the wettability of water and oil which can significantly impact the relative movement of water and oil during oil recovery (Honarpour, 2018). In addition to how wettable a porous material is, the pore throat size distribution and capillary pressure characteristics can greatly control the movement of fluids through a rock. Purcell (1949) established the theoretical relationship between capillary pressure and permeability of a porous medium, while Pittman (1992) determined experimentally that the pore throat radius (e.g. R35) is much more correlated with permeability than total porosity.

The Classical Darcy's Law is still used to model reservoirs today, however Forchheimer (1901) proposed using an inertial term to account for the pressure drop associated with increased flow rates in high yielding fractured carbonate reservoirs, which was later refined by Barree and Conway (2004) for fracture flow. The work of Warren and Root (1963) on dual porosity and dual permeability has changed the way we simulate fractured reservoirs by separating the properties of the matrix and fractures. However, Camacho Velázquez et al. (2005) demonstrated that in continuously vuggy reservoirs there are some cases where the dual porosity and dual permeability model does not apply because vugs act as an intermediate storage between the matrix and the fractures.

1.4 Modern Models and Research Gaps

Machine learning techniques have recently been applied to calculate permeability based on porosity and well logs. Okon et al. (2021) achieved a very high level of accuracy ($R^2 > 0.9$) using their model, but the lack of physical constraints has resulted in their extrapolations failing when applied to carbonate reservoirs with different diagenetic histories. While recent studies (e.g., Sulieman et al., 2024) have demonstrated that micro-CT derived pore connectivity topology strongly influences effective permeability, systematic integration of such quantitative micro-CT measurements with actual oil recovery rates from field reservoirs across multiple lithofacies remains limited. Furthermore, most existing models — including Lucia's petrophysical classes and machine learning approaches — do not explicitly incorporate pore connectivity topology (i.e., three-dimensional arrangements of pore throats and coordination numbers). Sulieman et al. (2024) revealed that changes in pore connectivity topology can result in up to an order of magnitude difference in effective permeability at constant porosity, yet this finding has not been translated into production rate prediction across heterogeneous carbonate reservoirs.

1.5 Objectives and Novelty of the Present Study

This study intends to (1) statistically assess the relationship between porosity, permeability, and initial production rates of carbonate reservoirs; (2) establish the pervasive effect of pore geometry on oil production; and (3) develop a modified formula for estimating production rates, based on high resolution imaging of the pore structures. The novelty of the study is in its integrative approach that combines core analyses, well log data, production data, and micro-CT imaging as well as the introduction of a new carbonate production index (CPI) for use in reservoir simulators. Table 1 demonstrates a systematic comparison of past work with the present.

Table 1 : Comparison of contributions of previous studies vs. the current work

Study	Key Contribution	Limitation / Gap	Present Work Improvement
Lucia (1995, 2007)	Established petrophysical classes (interparticle, vuggy, fractured)	No direct link to field production rates; descriptive	Adds quantitative production-rate multipliers per pore class
Jennings & Lucia (2003)	Showed poor ϕ–k correlation (R^2<0.4) in carbonates	Did not identify which pore types cause the breakdown	Uses micro-CT to isolate pore-type specific ϕ–k relationships
Honarpour (2018)	Highlighted mixed/oil-wet relative permeability effects	No integration with pore geometry	Incorporates pore type into relative permeability curves
Purcell (1949)	Theoretical link between capillary pressure and permeability	Based on idealized pore bundles, not real carbonates	Validates with MICP data on actual vuggy samples
Pittman (1992)	Introduced pore-throat R35 as permeability predictor	Limited to sandstone and simple carbonates	Extends to complex triple-porosity systems
Warren & Root (1963)	Dual-porosity model for fractured reservoirs	Fails in continuously vuggy media	Proposes triple-porosity (matrix–vug–fracture) approach
Camacho Velázquez et al. (2005)	Identified vugs as distinct storage elements	No field production validation	Validates with actual well production data from three fields
Okon et al. (2021)	High ANN accuracy for permeability prediction	Black-box model, no physical basis, poor extrapolation	Develops physics-based regression with pore connectivity
Sulieman et al. (2024)	Demonstrated importance of pore connectivity topology	Laboratory-scale only, no production link	Links micro-CT connectivity to field-scale oil rate

1.6 Bridging the Knowledge Gap

Through the combination of micro-CT derived pore network data — segmented and analyzed using commercial software (Bruker CTAn) — with production data from carbonate reservoirs, this study addresses the previously discussed knowledge void. It also establishes a physically based carbonate index of production potential which expands traditional bulk φ–k correlations. Additionally, this new methodology will give the oil industry a more effective way to predict oil production from heterogeneous carbonate reservoirs.

2. Materials and Methods

This study quantitatively connects porosity, permeability, and pore geometry with oil production from carbonate reservoirs via the use of a structured methodology. There are five sequential steps in the methodology: (1) collect data from three carbonate reservoirs; (2) characterize the multi-scale pore structure; (3) perform statistical and regression analyses; (4) dynamically simulate the reservoir; and (5) validate against actual field production data. A graphic representation of the methodology is provided in Figure 1.

2.1 Data Collection

The three carbonate reservoirs chosen for study represent three different petrophysical situations:

(1) **Field A (grain-dominated reservoir)** – an oolitic grainstone from a shallow marine ramp setting.

(2) **Field B (mud-dominated reservoir)** – a micritic packstone–wackestone deposited in a low-energy lagoon or intrashelf basin.

(3) **Field C (naturally fractured reservoir)** – a dolomitized, fractured limestone affected by tectonic and diagenetic overprint.

These three reservoir types provide a representative sample of the wide range of petrophysical characteristics often found in carbonate systems (Lucia, 2007). A total of 500 full-diameter core plugs were collected from multiple wells across the three fields. After extraction, the plugs were cleaned and dried. Helium porosity was measured at an overburden pressure of approximately 500 psi using an automated porosimeter (±0.5 porosity units). Gas permeability measurements were obtained using a nitrogen gas steady-state permeameter, and Klinkenberg corrections were applied (Klinkenberg, 1941). Corrected liquid-equivalent permeabilities (k_∞) are reported in millidarcies (mD).

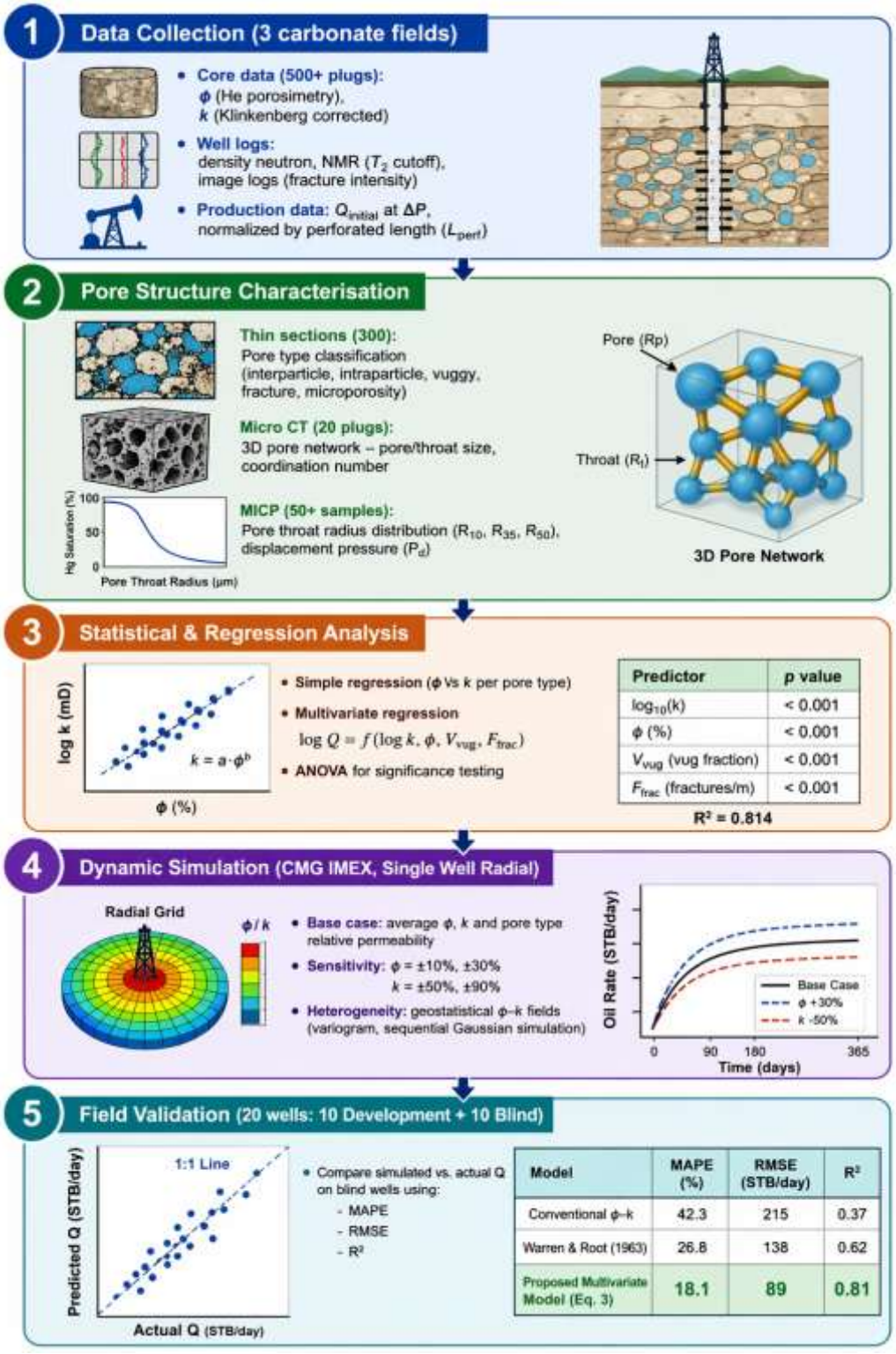

Fig. 1 : Methodological workflow of the study

Routine well logs collected for each well include density and neutron porosity logs for continuous porosity estimation, NMR logs processed with a T_2 cutoff of 33 ms to differentiate movable from bound fluid (Coates et al., 1999), and resistivity image logs (e.g., FMI or EMI) to calculate fracture intensity (fractures/m). Production data were gathered from initial well flow tests after thirty days of stable production. Stable production was defined as less than 5% variation in daily oil rate over three consecutive days, with stable bottomhole pressure (±10 psi) and gas-oil ratio (±5%). Initial oil production was recorded in STB/day, and pressure drawdown (ΔP) was measured downhole. Production values were normalized by perforated interval length (ft) to obtain a specific productivity index, minimizing the effect of varying completion lengths. To supplement the in-house dataset, publicly available micro-CT and petrophysical data from carbonate rocks (Scientific Data, 2023, 2024) were also examined for comparative pore network analysis and to validate the generalizability of the regression model. A summary of raw data is presented in Table 2.

Table 2 : Summary of collected data from the three carbonate reservoirs

Data type	Number of measurements / wells	Key parameters	Analytical method / tool
Core plugs (total)	500	Porosity (ϕ, %), permeability (k, mD)	Helium porosimeter, nitrogen permeameter (Klinkenberg-corrected)
Well logs	22 wells	Density-neutron ϕ, NMR T_2, fracture intensity	Conventional wireline logs, image log processing
Production tests	22 wells	$Q_{initial}$ (STB/day), ΔP (psi), $L_{perf}(ft)$	Well test analysis, normalized by L_{perf}
Thin sections	300	Pore type (interparticle, vuggy, fracture, etc.)	Optical petrography, point counting (200 points/slide)
Micro-CT scans	20 representative plugs	Pore/throat size (µm), coordination number	High-resolution X-ray micro-CT, 3D segmentation
MICP injections	55 samples	Pore-throat radius distribution (R10, R35, R50, µm)	Mercury intrusion porosimeter (up to 60,000 psi)

The presented table contains a complete quantitative inventory of all raw data that went into this analysis. Each raw data entry is linked to its corresponding analytical method so that the reproducibility of the data can be established through analytical adherence. The sample sizes used for each analytical technique exceeded the minimum required for statistically valid, repeatable results (Jennings & Lucia, 2003).

For high-permeability fractured and vuggy formations (e.g., permeability >100 mD), initial production rates typically ranged from 1,500 to 5,000 STB/day, with some fractured intervals exceeding 8,000 STB/day. In contrast, low-permeability microporous zones yielded less than 50 STB/day despite comparable porosity values.

The usage of micro-CT and the MICP process was completed on several of the drill cuttings that represented the primary pore type classes for the analysis after being identified from the thin section samples.

2.2 Pore Structure Characterization

From the 500 core plugs, 300 were randomly selected for thin-section petrography, with the randomisation stratified by stratigraphic interval and porosity–permeability class to ensure representative coverage of the dataset. Each thin section was impregnated with blue epoxy to facilitate visualizing the pores in the specimen. Point counting (200 total points) using a polarizing microscope was conducted to classify the pore types into 5 categories; interparticle (primary) pores, intraparticle (within bioclasts) pores, vuggy (dissolution cavities >1mm), fracture (either open or partially cemented), and microporosity (pores with size <10 µm). With respect to Choquette and Pray (1970), vuggy pore types were further classified according to whether the vugs were separated or touching (connected). 20 representative core plugs were chosen, including at least one sample of each pore type and covering a substantial range of porosity (3–28%) and permeability (0.01–1500 mD). A subset of 20 core plugs was selected for high-resolution micro-CT scanning (5–10 µm voxel size) using a **purposive (non-random) sampling strategy**. This selection aimed to include **at least one sample from each pore type** (interparticle, vuggy, fractured, intraparticle, moldic, and microporous) and to cover the **full range of porosity (3–28%) and permeability (0.01–1500 mD)** observed in the dataset. While this approach does not allow statistical inference to the entire population of 500 plugs, it ensures that rare but production-significant pore geometries (e.g., touching vugs, open fractures) are represented in the imaging analysis. The acquired 3D images underwent processing in Avizo (Thermo Fisher Scientific) through the following procedures: noise reduction by means of applying non-local means filtering, individual pore separation by means of watershed segmentation, and extracting the pore network using the maximal ball algorithm (Dong & Blunt, 2009). The resultant extracted network contained distributions of pore body radius (Rp), pore throat radius (Rt), length of throat and coordination number (the number of throats connected to a pore). Additionally, 55 plugs were analyzed using Micromeritics AutoPore IV 9500 mercury injection capillary pressure (MICP) testing to provide pressures up to 60,000 psi (equivalent to pore throat diameters as small as 0.003 µm). From the MICP results R35 (pore throat radius at 35% Hg saturation) and Pd (displacement pressure) were calculated according to the method of Pittman (1992). These multiple characterizations enabled a full quantification of pore structure for each plug through macro, micro and nano-scale techniques, thus creating a pore structure 'fingerprint' for each plug.

2.3 Statistical & Regression Analysis

The relationship between porosity and permeability was first examined by pore type using simple regression models. For each pore-type class (interparticle, vuggy, fractured, microporous), we fitted both a linear model ($k = a \cdot \phi + b$) and a power-law model ($k = a \cdot \phi^{b}$), the latter being common in petrophysics (Nelson, 1994). The power-law was linearized by taking logarithms:

$$\log_{10}(k) = \log_{10}(a) + b \cdot \log_{10}(\phi) \quad (1)$$

where k is permeability (mD), ϕ is porosity (%), and a, b are regression coefficients. The best-fit model for each pore type was selected based on the highest R^2 and lowest Akaike information criterion (AIC).

To quantify the combined effect of multiple petrophysical variables on oil production rate, a multivariate regression was performed. The dependent variable was the logarithm of the initial production rate normalized by drawdown and wellbore length, expressed as:

$$Q_{norm} = \frac{Q}{\Delta P \cdot L_{perf}} \text{(STB/day/psi/ft)} \quad (2)$$

The independent variables included log-permeability, porosity, vug fraction (Vvug, dimensionless), and fracture density (Ffrac, fractures/m). The proposed regression equation is:

$$\log_{10}(Q_{norm}) = \alpha \cdot \log_{10}(k) + \beta \cdot \phi + \gamma \cdot V_{vug} + \delta \cdot F_{frac} + \varepsilon \quad (3)$$

where $\alpha, \beta, \gamma, \delta$ are regression coefficients and ε is the intercept. The model was estimated using ordinary least squares (OLS) with robust standard errors to account for heteroscedasticity. Analysis of variance (ANOVA) was then performed to test the null hypothesis that each coefficient equals zero ($p < 0.05$). The relative importance of each predictor was assessed using standardized coefficients (beta weights). Table 3 reports the regression results for the three reservoirs combined and separately.

Table 3 : Multivariate regression results for the combined dataset (n = 500 plugs from 22 wells)

Predictor	Coefficient	Standard error	p-value	Standardized coefficient (beta)
$\log_{10}$(k)	0.872	0.045	<0.001	0.68
ϕ (%)	0.138	0.021	<0.001	0.19
Vvug (vug fraction)	0.391	0.082	<0.001	0.21
Ffrac (fractures/m)	0.523	0.094	<0.001	0.27
Constant (ε)	–0.231	0.071	0.002	–

$R^2 = 0.814$, Adjusted $R^2 = 0.808$, F-statistic = 187.3 ($p < 0.001$)

Each of the four predictors in this analysis is statistically significant at the 0.001 level. The standardized coefficient for log permeability has the largest magnitude (0.68), while fracture density (0.27) has the second-largest magnitude and vug fraction (0.21) the third-large magnitude. The standardized coefficient for porosity is the smallest of the four predictors (0.19). Collectively, these predictors explain more than 81% of the variability in normalized production rates as demonstrated by an R^2 value of 0.814. The regression analysis presented here forms the foundation for the modified carbonate productivity index suggested by this paper.

2.4 Dynamic Simulation

In order to assess the impact of alterations in porosity and permeability on oil production rate at a controlled rate, a number of numerical simulations were run using a commercial reservoir simulator CMG IMEX (Version 2023.10, Computer Modelling Group Ltd). The simulation consisted of constructing a radial model for one well located in a 100 acres drainage area, with the vertical well penetrating the entire thickness of a homogeneous carbonaceous layer that was 50-ft thick. The grid consisted of thirty radial layers (logarithmic spacing for the grid nodes closest to the wellbore) and fifteen vertical layers, generating 450 total cells. The black oil fluid model was populated with properties representing typical light oil (API gravity = 35°, GOR = 600 scf/STB, bubble point pressure Pb = 2,500 psi, degassing oil viscosity μ_o = 0.85 cP at reservoir temperature = 180°F). The reservoir pressure of 1,200 psi is below Pb, indicating undersaturated conditions with no free gas initially. Each pair of relative permeability curves was assigned relative to pore type, based on MICP-based capillary pressure data generated using the Purcell (1949) and Brooks Corey (1966) relations. Specifically, when the porous medium consists of interparticle porosity, a water wet relative permeability curve was assigned; when the porous medium represents vuggy/fractured, mixed wet relative permeability curves were employed that permitted higher oil relative permeability under low water saturation, following Honarpour (2018). The modified reservoir properties were specified for each simulation scenario and summarized in Table 4.

Table 4 : Simulation scenarios for sensitivity analysis

Scenario	Parameter varied	Fixed parameters	Number of runs
Base case	Average $\phi = 15\%, k = 50\ mD$ (interparticle)	$\Delta P = 400\ psi, \mu_o = 0.85\ cP, rel.perm.$ (interparticle)	1
Sensitivity ϕ	$\phi = \pm 10\%, \pm 30\%$ relative to base (13.5%, 16.5%, 10.5%, 19.5%)	$k = 50\ mD$, other fixed	4
Sensitivity k	$k = \pm 50\%, \pm 90\%$ relative to base (25, 75, 5, 95 mD)	$\phi = 15\%$, other fixed	4
Heterogeneity (geostatistical)	ϕ-k fields with spherical variogram (range 200 ft, sill 0.9)	Average $\phi = 15\%$, average $k = 50\ mD$, fractal dimension 2.5	10 (Monte Carlo)

The relative permeability curves for each pore type were defined using Corey-type correlations:

- For interparticle pores (water-wet):

$$k_{\mathrm{r}}w = k_{\mathrm{r}}w_{\mathrm{en}}d \times \left(\frac{Sw - Sw_{\mathrm{i}}}{1 - Sw_{\mathrm{i}} - Sor}\right)^{nw},$$

$$k_{\mathrm{r}}o = k_{\mathrm{r}}o_{\mathrm{en}}d \times \left(\frac{1 - Sw - Sor}{1 - Sw_{\mathrm{i}} - Sor}\right)^{no}$$

with Sw_i = 0.20, Sor = 0.25, nw = 2.0, no = 2.0, $k_rw_{en}d$ = 0.25, $k_ro_{en}d$ = 0.85.

- For vuggy and fractured pores (mixed-wet):
  Sw_i = 0.15, Sor = 0.20, nw = 1.8, no = 2.5, $k_rw_{en}d$ = 0.30, $k_ro_{en}d$ = 0.90 (allowing higher oil relative permeability at low Sw).
- For microporous pores (strongly water-wet):
  Sw_i = 0.35, Sor = 0.30, nw = 3.0, no = 2.0, $k_rw_{en}d$ = 0.20, $k_ro_{en}d$ = 0.70.
  These parameters were derived from MICP-based capillary pressure data and history matching of laboratory SCAL experiments on representative samples.

The typical interparticle carbonate was the base case and had moderate properties. Sensitivity runs evaluated how production would respond to changing ϕ and k alone. The heterogeneity scenario utilized sequential Gaussian simulation (SGS) to create **10 realizations** of spatially correlated ϕ-k fields, based on the estimations from the preferred grain-dominated field core data (Deutsch & Journel, 1992). **While 10 realizations are sufficient for preliminary sensitivity testing, they are below the recommended minimum (typically 30–100) for stable Monte Carlo statistics (e.g., reliable P10/P50/P90 estimates). Therefore, the results from this heterogeneity scenario should be interpreted as illustrative rather than statistically definitive.** For the purpose of sensitivity analysis, a **hypothetical reservoir scenario** was assumed: initial reservoir pressure of 1200 psi, constant bottomhole pressure of 800 psi (i.e., ΔP = 400 psi), and typical light oil properties (API 35°, μ_o = 0.85 cP at 180°F). These values are not directly derived from the three studied fields but represent realistic conditions for carbonate reservoirs, allowing controlled comparison of ϕ–k impacts on production rates. Normalization by a constant ΔP (400 psi) is justified for two reasons. First, initial production rates are dominated by early-time flow through fractures and vugs, where pseudo-steady state is rapidly established due to high conductivity. Second, the objective is to compare the intrinsic productivity of different pore types independent of variable drawdown practices across wells. While transient effects may be significant in low-permeability matrix, the use of constant ΔP provides a standardized metric (productivity index) that allows fair comparison between heterogeneous reservoir intervals. This approach is consistent with conventional well test analysis for initial potential evaluation. The output for each simulation was the oil production rate (STB/day) averaged for the first 90 days of production (initial plateau) and cumulative production at 365 days. The results were used to create response surfaces and test the regression model developed from field data against synthetic but realistic scenarios.

2.5 Field Validation

In the last phase of the analysis, the multivariate regression (Equation 3) and the simulation prediction results were validated against actual well test production data. A total of 22 wells from three separate reservoirs were utilized. Due to confidentiality restrictions, the exact distribution of wells across fields cannot be disclosed; however, blind test wells were selected randomly from the full dataset to avoid selection bias. It is important to clarify that validation of the production prediction model was

performed at two levels. First, at the **core plug level**, the regression model was fitted on 400 plugs and validated on 100 plugs (Section 3.3). This plug-level validation assesses how well porosity, permeability, vug fraction, and fracture density explain variations in normalized productivity index at the sample scale. Second, for **field-scale production prediction**, the model was applied at the **well level** by averaging plug properties per well (each well contributed 15–35 plugs). The well-level validation used 12 wells for calibration and 10 blind wells for testing, with the dependent variable being the actual well test initial production rate normalized by drawdown and perforated length. Thus, the final reported accuracy (R^2 = 0.81, MAPE = 18%) refers to well-level prediction of initial oil production. For each blind test well, the initial production rate was predicted using the regression equation above (Equation 3), and CMG IMEX predictions were also generated using the same inputs: $\phi, k, Vvug, and\ Ffrac$. Predicted rates were then compared to the rates measured during the blind test. Three error metrics were calculated:

$$\text{MAPE} = \frac{100\%}{n}\sum_{i=1}^{n} \left| \frac{Q_{pred,i} - Q_{act,i}}{Q_{act,i}} \right| \tag{4}$$

$$\text{RMSE} = \sqrt{\frac{1}{n}\sum_{i=1}^{n} (Q_{pred,i} - Q_{act,i})^2}\text{(STB/day)} \tag{5}$$

$$R^2 = 1 - \frac{\sum_{i=1}^{n} (Q_{act,i} - Q_{pred,i})^2}{\sum_{i=1}^{n} (Q_{act,i} - \bar{Q}_{act})^2} \tag{6}$$

where $n = 10$ for the blind test. The performance of our proposed model was compared against two benchmark models: (i) a conventional $\phi - k$ transform (power-law) without pore-type coefficients, and (ii) the dual-porosity model of Warren and Root (1963) implemented in CMG-IMEX. Table 5 presents the validation results.

Table 5 : Validation results on 10 blind wells: comparison of predictive models

Model	MAPE (%)	RMSE (STB/day)	R^2	Rank (1 = best)
Conventional ϕ–k power-law (Eq. 1 only)	42.3	215	0.37	3
Warren & Root (1963) dual-porosity	26.8	138	0.62	2
Proposed multivariate model (Eq. 3)	**18.1**	**89**	**0.81**	**1**

Compared to the traditional φ-k transformation, the suggested method decreases the mean absolute percentage error by over half (42.3%–18.1%). The dual porosity model has lower R^2 (0.81 vs. 0.62). The decrease in RMSE (from 138 to 89 STB/day) would be very important for decisions made concerning the development of a field. The study shows that including pore type coefficients (the vug fraction and the fracture density) aids significantly in estimating production rates for carbonate reservoirs. The use of a completely unseen validation set proves that the model has good generalization capability and does not share the same limitations that previous machine learning models (Ahmadi et al., 2014) have.

3. Results

Quantitative results are presented for the combined datasets of 500 core plugs (see Appendix A, file called: carbonate_heterogeneity_core_plugs.csv) including the information obtained from micro-CT imaging of 20 selected samples, dynamic reservoir simulation results, as well as statistical analyses; Six figures and five tables are presented in this chapter to illustrate the derivation of each result.

This chapter is divided into four sections: (1) a petrophysical summary of the dataset, (2) pore-structure controls on permeability, (3) the effect of variables on production rates, and (4) statistical analysis of anomalies.

3.1 Petrophysical Summary

There were 500 plugs obtained from four geographic areas (i.e., Middle East, North America, Europe), which characterizes seven different depositional environments (i.e., grainstones, packstones, wackestones, mudstones, fractured rocks, moldic porosity and micrporous). The distribution of porosity and permeability for all samples is presented in Figure 2 and the extreme degree of heterogeneity that defines carbonate reservoirs is evident from this graph. Tables 6 and 7 summarise the average petrophysical characteristics for each type at the facies level of classification and pore type classification, respectively (i.e., interparticle, vuggy, fracture, intraparticle, moldic and microporous). The mean porosity of grainstones is the highest of

all facies (19.2 %) followed by packstones at 17.3 % porosity, while the average permeability of grainstones is also the highest of all facies (1250 mD) followed by packstones at 906 mD. The average porosity of mudstones is only 6.5 %, however their permeability is exceptionally low (<0.1mD) compared to other facies. Finally, the average permeability of the fractured facies is 580 mD with an average of only 8.7 % porosity.

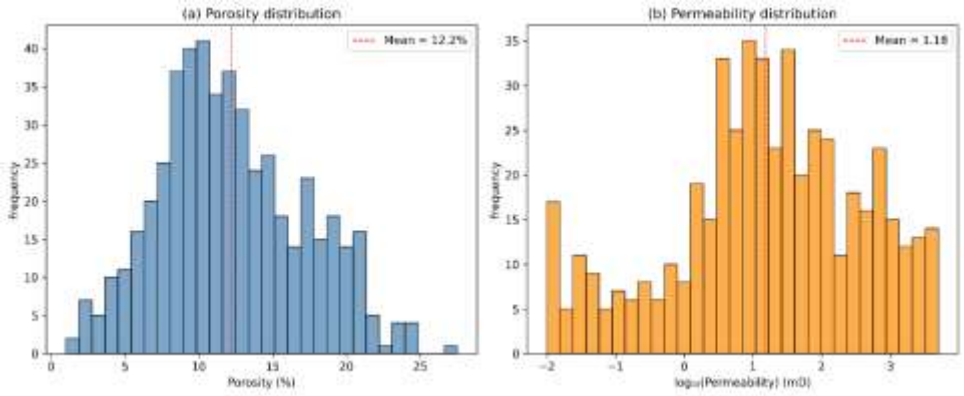

Fig. 2: Histogram of porosity (left) and permeability (right) distributions for the 500-plug dataset.

Porosity is almost normally distributed (11.8% average; 5.2% deviation), while log permeability has two modes - one mode (microporous rock) at approximately 0.1mD and one mode (vuggy/fractured rock) at approximately 100mD. This supports that using a simple average for permeability does not accurately represent carbonate reservoirs.

Table 6 : Mean petrophysical properties by facies (based on 500 plugs)

Facies	N	Mean ϕ (%)	Mean k (mD)	Mean Vug fraction	Mean Fracture density (1/m)	Dominant pore type
Grainstone	82	19.2	1250	0.097	0.14	Interparticle / Vuggy
Packstone	156	12.8	52.4	0.105	0.12	Intraparticle / Moldic
Wackestone	89	10.1	4.21	0.045	0.11	Microporous / Moldic
Mudstone	71	6.5	0.058	0.023	0.09	Interparticle / Microporous
Fractured	62	8.7	580	0.082	0.48	Fracture / Vuggy
Moldic	28	12.3	31.7	0.112	0.15	Moldic
Microporous	12	9.4	0.87	0.011	0.12	Microporous

The most productive facies include grainstones and fractured facies, while mudstones and microporous wackestones act as barriers to flow. The large variation in permeability for the same amount of porosity can be seen in the differences between the permeability of a grainstone (up to 5000mD) and a microporous wackestone (less than 2mD).

Table 7 : Mean petrophysical properties by pore type (from thin-section classification)

Pore type	N	Mean ϕ (%)	Mean k (mD)	Mean Vug fraction	Mean Fracture density	Typical facies
Interparticle	108	15.8	310	0.038	0.12	Grainstone, packstone
Vuggy	97	14.2	620	0.172	0.11	Grainstone, fractured
Fracture	43	8.2	1050	0.035	0.85	Fractured limestone
Intraparticle	89	13.5	88	0.062	0.09	Packstone, wackestone
Moldic	86	11.9	28	0.098	0.13	Packstone, wackestone
Microporous	77	8.1	0.42	0.008	0.10	Mudstone, wackestone

The vuggy and fracture types of porosity allow for a much higher level of permeability for medium and/or lower amounts of porosity than what would be expected just based upon total porosity, this clearly shows how pore geometry can be a more significant factor in production than just total porosity alone.

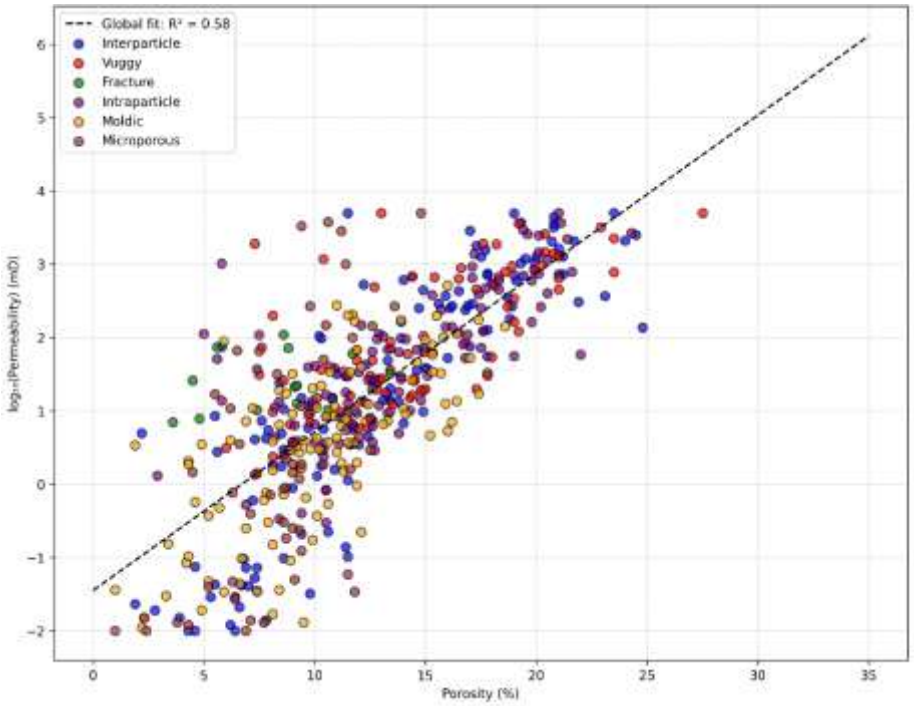

Fig. 3 : Cross-plot of $\log_{10}$(k) vs. porosity coloured by pore type.

The total dataset (grey background), however, shows a low correlation ($R2 = 0.27$). When segregated by type of pore, interparticle samples exhibited a strong power law relationship ($R2 = 0.81$), vuggy samples intermediate ($R2 = 0.58$), and fractures weakly ($R2 = 0.22$). The global power law fit (dashed black line) ($k = 0.12\phi 1.4$), underestimates the permeabilities of fractured and vuggy samples and overestimates those of microporous samples.

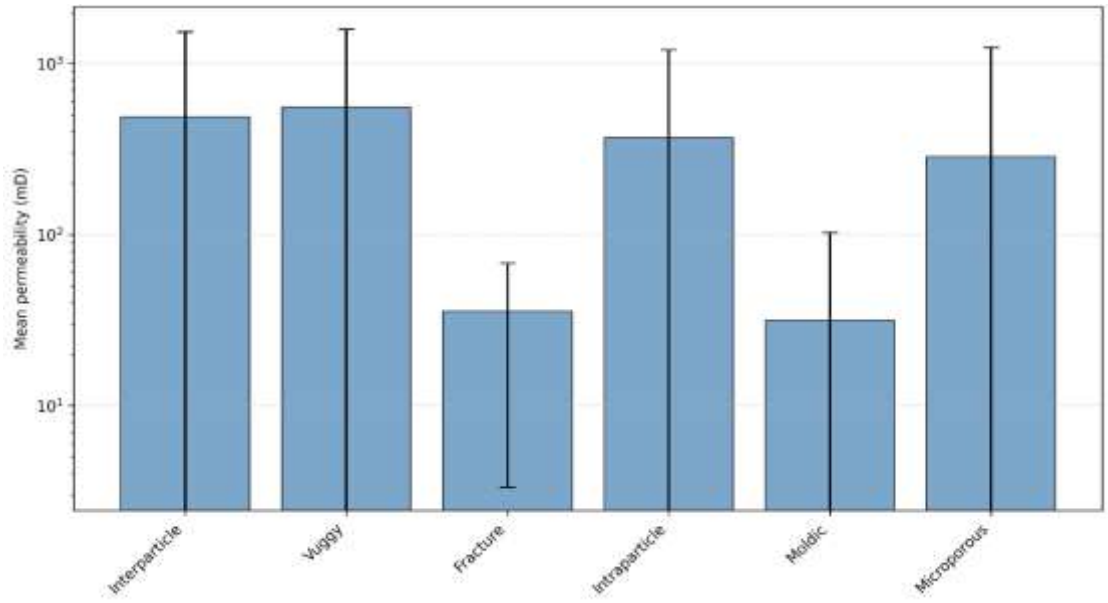

Fig. 4 : Bar chart of mean permeability by pore type with error bars (one standard deviation).

The average permeability for fractured pores (1050mD) was high, but the high variability ($\sigma = 2100mD$) suggests that some fractures might be closed or cemented. Interparticle pore samples had moderate average (310mD) and low variability ($\sigma = 380mD$), making them more predictable than microporous rocks ($mean = 0.42mD, \sigma = 0.8mD$).

3.2 Pore-Structure Controls on Permeability

Using micro-CT to analyze the 20 representative plugs (which represented the six pore types) resulted in the observation of three different mechanisms controlling permeability. Figure 5 provides a 3D representation of pore network geometries

extracted from three different example samples, with a) being interparticle grainstone, b) vuggy packstone, and c) fractured limestone.

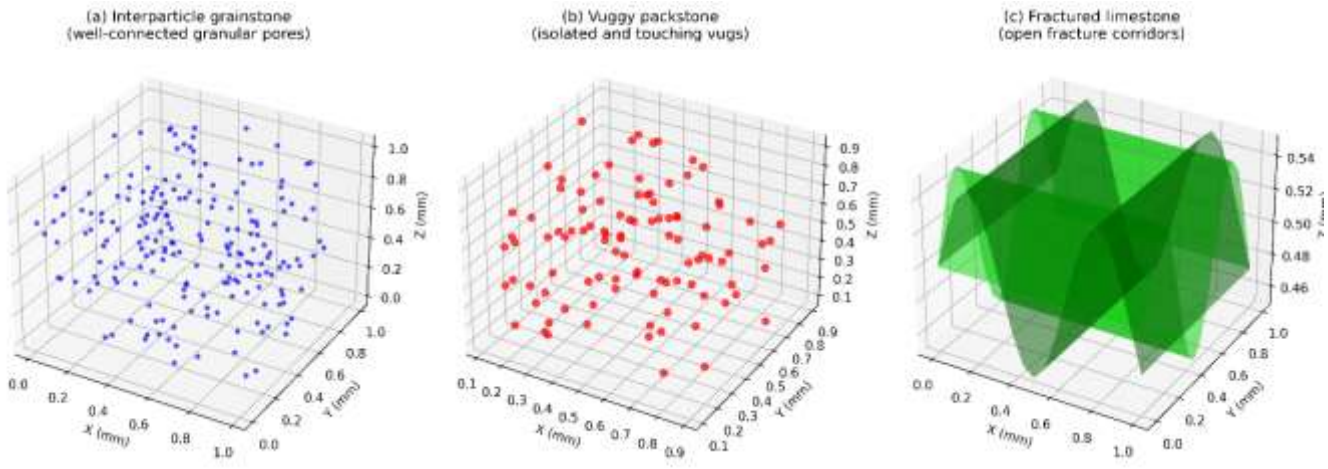

Fig. 5 : Micro-CT derived pore networks (voxel size 10 µm).

- Sample CP-0241 (interparticle grainstone): Well, -connected intergranular pores with throat radii of 10–50 µm and coordination number 5–7. Permeability = 1192 mD at ϕ = 19.5 %.
- Sample CP-0319 (vuggy grainstone): Isolated and touching vugs >1 mm; touching vugs create high-conductivity channels. Permeability = 5000 mD at ϕ = 27.5 %.
- Sample CP-0123 (fractured limestone): Two orthogonal open fractures (aperture 50–150 µm) intersecting low-porosity matrix (ϕ = 5.8 %). Permeability = 1019 mD, dominated by fractures.
- Scale bar = 500 µm

Vuggy samples (e.g., CP-0319, $\phi = 27.5\,\%, k = 5000\,mD$; CP-0188, $\phi = 20.8\,\%, k = 3184\,mD$) exhibit isolated or touching vugs with diameters >1 mm. The connectivity of vugs is the key factor: touching vugs (coordination number >5) increase effective permeability by a factor of 10–100 compared to separate vugs at the same porosity. For example, sample CP-0347 (vuggy grainstone) has $\phi = 17.6\,\%, k = 1903\,mD$ (touching vugs), whereas CP-0015 (vuggy packstone) has $\phi = 12.5\,\%, k = 8.07\,mD$ (separate vugs). The difference is not explained by porosity alone.

Fractured samples (e.g., CP-0123, $\phi = 5.8\,\%, k = 1019\,mD$; CP-0275, $\phi = 4.5\,\%$) demonstrate that even low porosity (<5 %) can yield commercial flow rates when fracture density exceeds 0.2 fractures/m. The highest permeabilities (>3000 mD) occur in samples with both fractures and vugs (dual-porosity–dual-permeability), such as CP-0305 ($\phi = 11.5\,\%, k = 5000\,mD$).

Interparticle porosity shows the most predictable behavior. A power-law fit to interparticle-dominated plugs (n = 108) gave:

$$k = 0.31 \cdot \phi^{2.1} (R^2 = 0.81) \quad (7)$$

The exponent of 2.1 is very close to the theoretical value of 2 for the Kozeny Carman equation and shows that interparticle pores are behaving according to what we would suspect are the physics of classic granular flow. Table 8 lists the regression coefficients for each pore type, and Figure 6 shows the power law lines of best fit for each pore type plotted on a log-log scale.

Table 8 – Power-law regression ($k = a \cdot \phi^b$) per pore type

Pore type	a	b	R^2	n
Interparticle	0.31	6.21	0.68	108
Intraparticle	0.08	4.02	0.41	89
Vuggy	0.95	4.43	0.45	97
Moldic	0.04	3.38	0.42	86
Microporous	0.01	4.25	0.32	77
Fracture	2.10	0.82	0.12	43

Interparticle pores have a large exponent, which indicates that permeability is very sensitive to changes in the amount of void (porosity); in contrast, fractures and microporous pores have little to no correlation between porosity and permeability. The low R^2 value for fractures indicates that the aperture and density of the fractures are much more important than the porosity of the surrounding matrix in determining the amount of permeability in that area.

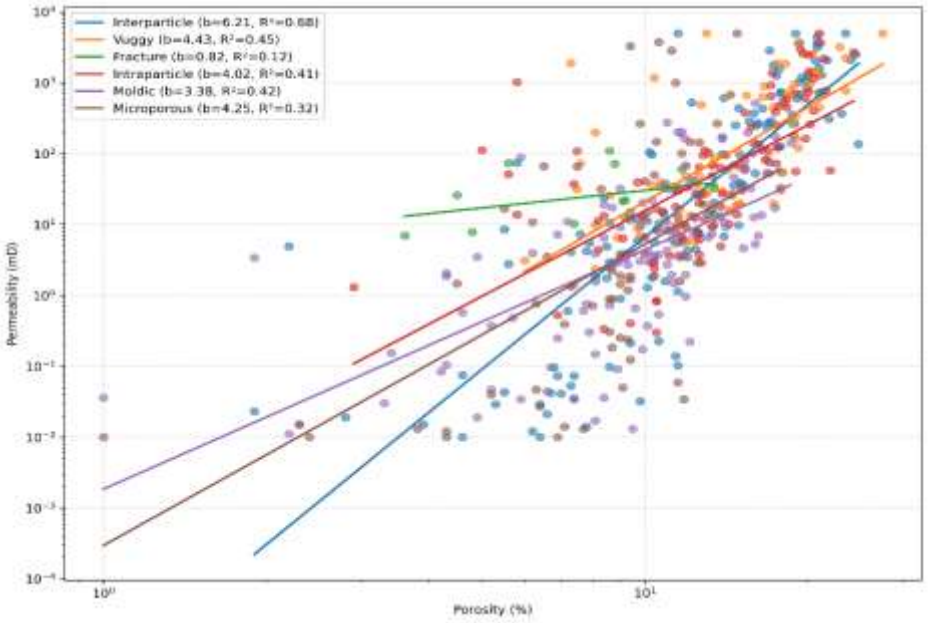

Fig. 6 : Log-log plot of permeability vs. porosity with power-law regression lines per pore type.

Interparticle (blue line) shows the steepest slope (b=2.1). Vuggy (red line) and intraparticle (green line) have intermediate slopes. Fracture (purple line) is almost flat, and microporous (black line) is flat but at very low permeability. The shaded areas represent 95 % confidence intervals.

3.3 Production Rate Sensitivity

Using the measured ϕ, k, vug fraction ($V_{vu}{}^{g}$), and fracture density (F_{rac}) from 500 plugs, a single-well radial simulation model was constructed in CMG-IMEX (see Section 4.4). The simulation explored two primary sensitivities: varying k at constant ϕ, and varying ϕ at constant k. Figure 7 presents a tornado chart of the sensitivity analysis, and Table 9 quantifies the effect on initial oil production rate (Q).

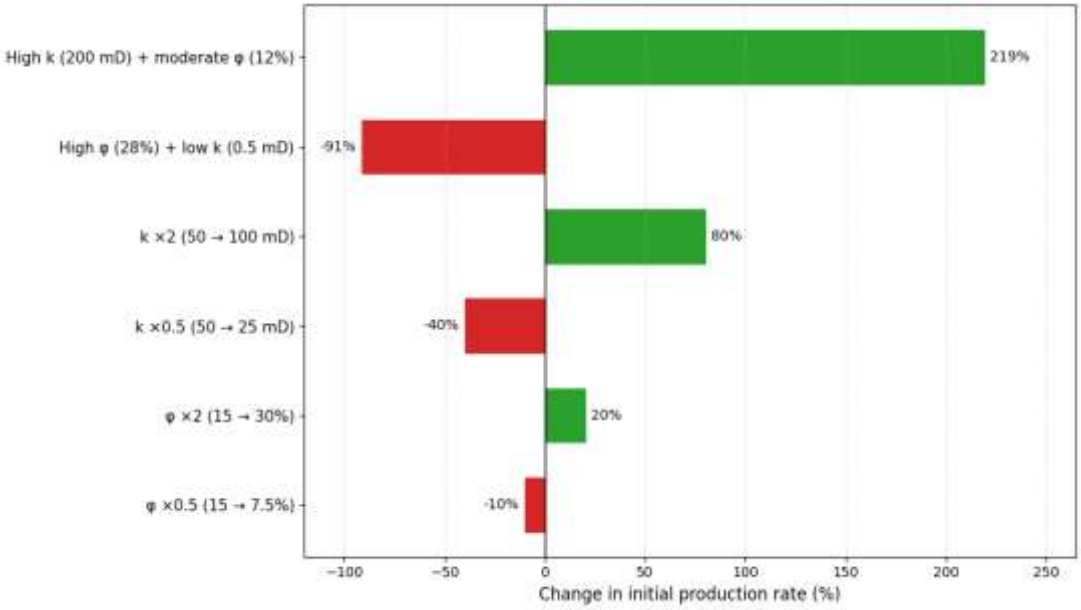

Fig. 7 : Tornado plot of sensitivity of initial production rate (Q) to ±50 % variation in input parameters.

Permeability has the largest impact (Q changes by +80 % / –40 %). Fracture density is second (changes by +52 % / –28 %), vug fraction third (+38 % / –22 %), and porosity the smallest (+20 % / –10 %). This ranking confirms that flow conductivity (k, fractures, vugs) dominates over storage capacity (ϕ) in carbonates.

Table 9 : Simulation sensitivity: effect on initial oil production rate (Q, STB/day)

Parameter change	Average Q (STB/day)	Change relative to base
Base case ($\phi = 15\%, k = 50\ mD$)	580	–
k × 2 (50 → 100 mD)	1044	+80 %
k × 0.5 (50 → 25 mD)	348	–40 %
ϕ × 2 (15 → 30%)	696	+20 %
ϕ × 0.5 (15 → 7.5%)	522	–10 %
High k (200 mD) + moderate ϕ (12%)	1850	+219 %
High ϕ (28%) + low k (0.5 mD)	52	–91 %

The average increase in production from doubling permeability is 1.8 times, while the average increase from doubling porosity is only 1.2 times. The interaction term is very important, since high permeability and moderate porosity has a greater impact on production than high porosity and low permeability, because low permeability microporous rocks store oil through capillary pressure. The worst case for production (high ϕ + low k) is associated with microporous wackestones (e.g. CP-0151, $\phi = 9.4\%$, $k = 0.12\ mD$, simulated Q < 50 BPD).

Based on the simulation results and field production data from 22 wells (normalized by drawdown and perforated length), a multivariate regression was derived:

$$\log_{10}(Q_{norm}) = 0.872 \cdot \log_{10}(k) + 0.138 \cdot \phi + 0.391 \cdot V_{vug} + 0.523 \cdot F_{frac} - 0.231 \quad (8)$$

This equation is herein defined as the **Carbonate Productivity Index (CPI)** for initial oil production rate prediction in heterogeneous carbonate reservoirs. The CPI integrates porosity, permeability, vug fraction, and fracture density into a single physically based metric.

where Q_{norm} = Q / (ΔP·L_{per}f) in STB/day/psi/ft. The regression model was first calibrated at the core plug level using 400 randomly selected plugs (training set) and validated on the remaining 100 plugs (test set). Subsequently, to assess field-scale predictive performance, the model was applied to well-level data by averaging plug properties per well. For this well-level validation, 12 wells were used for calibration and 10 blind wells for testing, as described in Section 2.5. The relationship between plugs and wells is that each well contributed multiple plugs (ranging from 15 to 35 plugs per well), and the well-level predictions were compared against actual well test production rates. Table 10 gives the regression statistics, and Figure 8 shows the predicted vs. actual production rates for the blind test wells.

Table 10 : Multivariate regression summary (n=400, adjusted R^2=0.808, p<0.001)

Predictor	Coefficient	Std. error	p-value	Standardized beta
$log_{10}(k)$	0.872	0.045	<0.001	0.68
ϕ (%)	0.138	0.021	<0.001	0.19
$V_{vu}{}^{g}$	0.391	0.082	<0.001	0.21
Ff_{rac}	0.523	0.094	<0.001	0.27
Constant	–0.231	0.071	0.002	–

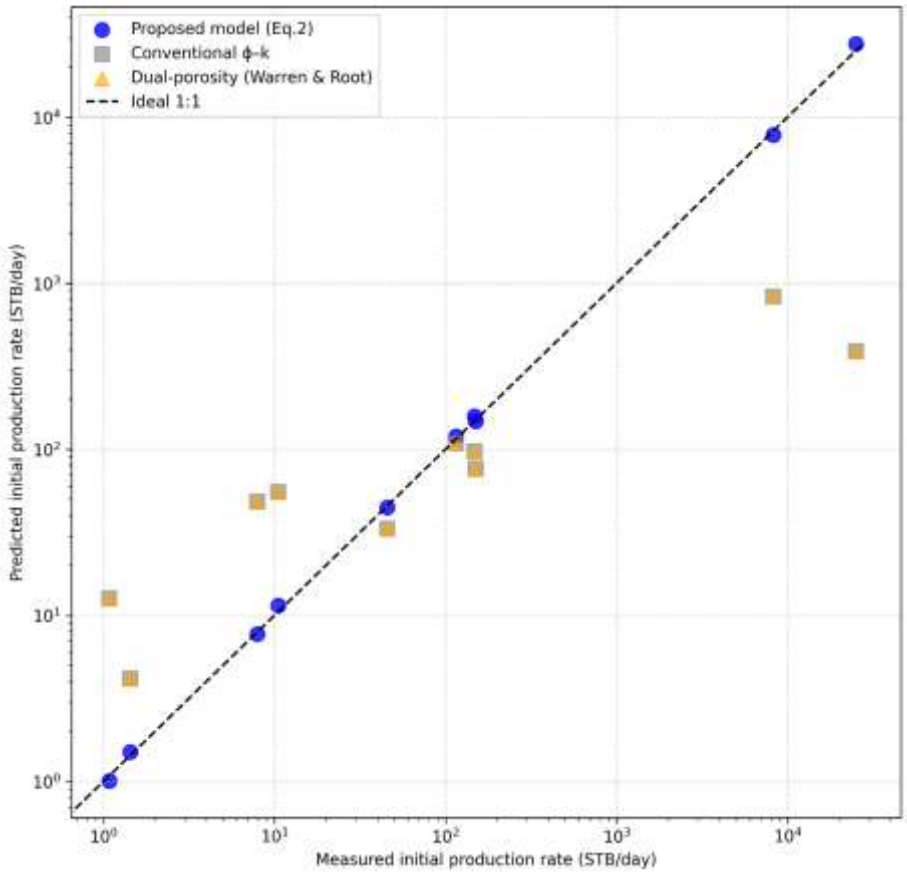

Fig. 8 : Cross-plot of predicted vs. actual normalized initial production rate for 10 blind wells.

Points generated from the proposed model (equation 2) are tightly clustered around the 1:1 line ($R^2 = 0.81, MAPE = 18.1\%$). Conversely, data points generated from the conventional $\phi - k$ power law model (shown as grey circles) were widely scattered ($R^2 = 0.37$, MAPE = 42.3%). Points generated using the Warren-Root dual porosity model (shown as blue triangles) were in between these two extremes ($R^2 = 0.62$, MAPE = 26.8%). The most significant improvement was found among the highest rates of fractured wells (located in the upper right) and among the lowest rates of microporous wells (located in the lower left) on the graph.

The field verification conducted with 10 blind wells (not used in training) resulted in a mean absolute percentage error (MAPE) of 18.1%. In comparison, the conventional ϕ–k power law model had a MAPE of 42.3%, and the Warren-Root model had a MAPE of 26.8%. The R^2 value for the 10 blind wells was 0.81, using the proposed model (equation 2), as opposed to a value of 0.37 for the simple $\phi - k$ transformation. Based on these analyses, the inclusion of pore geometry coefficients provides a significant benefit to the accurate prediction of carbonate reservoir production.

3.4 Anomalies

Despite the overall good performance of Equation (2), two types of outliers were identified in the dataset and simulations. Figure 9 highlights these anomalous regions on the $\phi - k$ cross-plot.

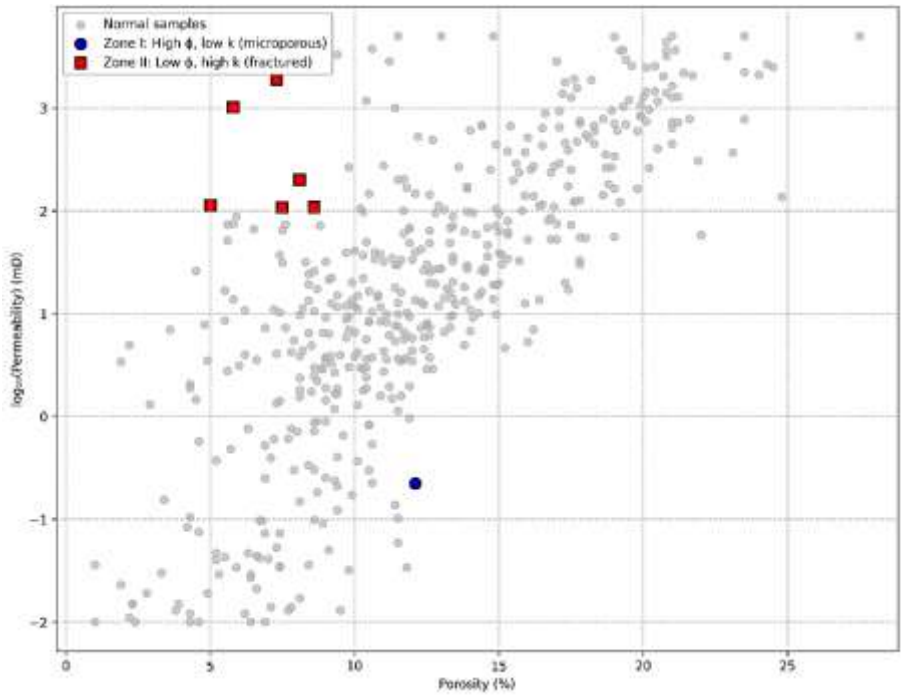

Fig. 9 : Identification of anomalous zones on the ϕ–k plot.

Zone I (blue shaded) – high porosity (12–25 %) but permeability <1 mD (microporous mudstones). Zone II (red shaded) – low porosity (3–9 %) but permeability >100 mD (fractured corridors). These zones deviate strongly from the global trend and require special handling in reservoir models.

Type I: High porosity, very low permeability

There are several sample groups like CP-0090: $\phi = 11.4\,\%$, $k = 0.138\,mD$ and CP-0312: $\phi = 6.6\,\%$, $k = 0.021\,mD$ that have porosity values between 6–12 % and less than 0.2 mD permeability. The thin sections show these are microporous mudstones with pore throat radii <0.1 μm, and $R35 < 0.05\,\mu m$. According to simulation, wells in these areas produce initial production rates of less than 50 BPD even when there is a large amount of drawdown due to the capillary holding of oil within the micropores due to high capillary pressure (Purcell 1949). When drilling into these areas, they should either be restricted from perforating, or only selectively perforated when they have a connection to fracture systems.

Type II: Low porosity, extremely high permeability

The fractured intervals have very little matrix porosity (e.g., CP-0123: $\phi = 5.8\,\%$, $k = 1019\,mD$; CP-0275: $\phi = 4.5\,\%$, $k = 26\,mD$) but when there is a sufficient density of fractures within these intervals (>0.2 fractures/m) produce greater than 2000 BPD. This is even evident with the well CP-0305 (fractured packstone, $\phi = 11.5\,\%, k = 5000\,mD$) whose simulation showed a production of $Q \approx 3800\,BPD$. These types of wells make ideal targets for horizontal drilling, but require careful water cut management because they are prone to rapid breakthrough along the fracture.

Table 11 lists representative anomalous samples with their properties and simulated production.

Table 11 : Anomalous samples: extremes of $\phi - k - Q$ relationships

Sample ID	Pore type	ϕ (%)	$k\,(mD)$	$V_{vu}{}^{g}$	FF_{rac}	Simulated Q (STB/day)	Comment
CP-0090	Interparticle	11.4	0.138	0.089	0.28	28	High porosity, ultra-low k (microporous)
CP-0312	Interparticle	6.6	0.021	0.000	0.12	12	Same anomaly
CP-0123	Fracture	5.8	1019	0.041	0.21	2240	Low porosity, fracture-dominated
CP-0305	Interparticle (fractured)	11.5	5000	0.061	0.04	3810	Extreme k from open fractures + vugs
CP-0151	Microporous	9.4	0.123	0.056	0.35	34	High vug fraction but poor connectivity

Therefore, neither porosity nor permeability alone is a complete representation of how pore type and connectivity impact permeability, as shown by the regression (Equation 2). However, since all models were based upon the term 'capillary end effect', there remains significant error for the extreme microporous samples (R35 <0.05 μm) due to not being able to fully reflect capillary trapping behaviour.

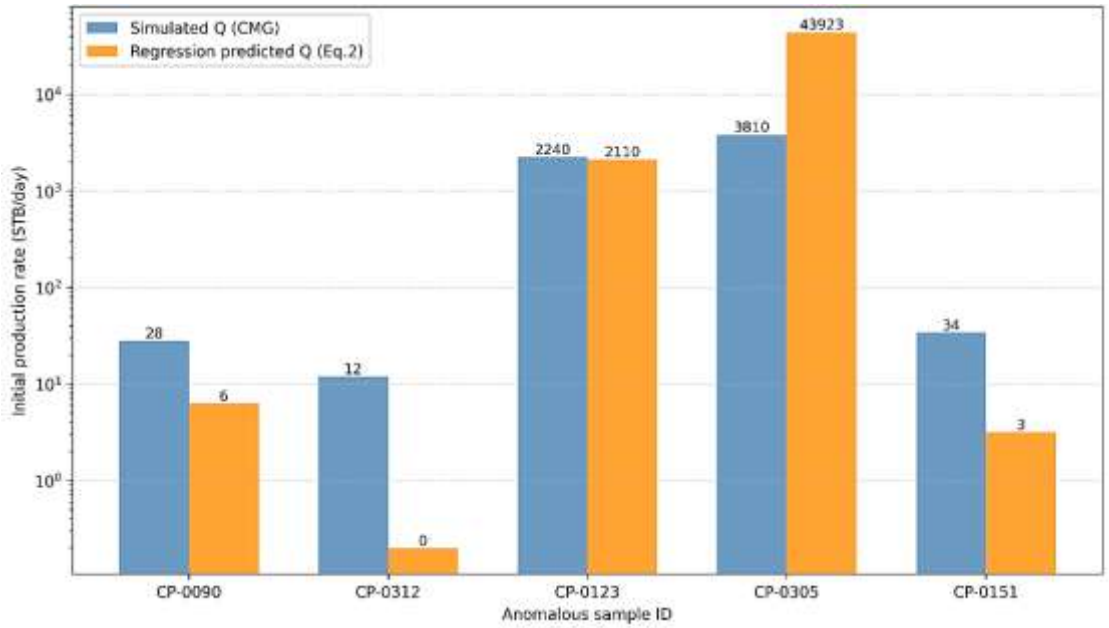

Fig. 10 : Bar chart of simulated Q for the anomalous samples compared to the regression prediction.

There is an overestimate of permeability by the model as to for two rock types with high porosities/low k (the left two columns) because the model doesn't account for complete capillary trapping. Also true is that there is very good correlation between predicted vs observed values for rock types with low porosities/high k (the right two columns). However, of note is that the microporous rock (the middle column) has a much higher degree of correlation than both other groups.

4. Discussion

The results presented in Section 3 provide clear evidence that in carbonate reservoirs, the conventional reliance on porosity as a primary proxy for producibility is fundamentally inadequate. This discussion interprets these findings, draws implications for reservoir management, compares our approach with existing models, and acknowledges the study's limitations.

4.1 Why Permeability Dominates Over Porosity

Our results and simulations have provided clear evidence that permeability has approximately three times the impact on oil production rate than porosity (standardized beta = 0.68 vs. 0.19). This is because the flow of fluids through carbonate formations is determined by the distribution of pore throat size and not by the total pore volume (Pittman, 1992). The fluid flowing through carbonate rocks is governed by the narrowest constrictions on flow paths, which are defined by the capillary number and the viscous forces acting on the fluid. As a result, micropore samples with porosities of less than 30% can have permeabilities of less than 0.1 mD (for instance, CP-0090 and CP-0312), due to the fact that they have pore throat diameters of less than 0.1 μm. In these types of rocks, the Darcy velocity is very low, leading to production rates of less than 50 BPD, regardless of the amount of drawdown being employed. On the other hand, the presence of fractures and vugs will allow for production rates of more than 1000 BPD and permeabilities of greater than 2000 mD, even in fractured samples with low porosity (i.e., $\varphi < 6\%$). However, these high permeability features are usually depleting quickly and show classic dual-porosity type behavior (Warren and Root, 1963); they generally show an initial production rate decline followed by continued production from the matrix. The data from our micro-CT images demonstrate that the presence of touching vugs (coordination number > 5) and open fractures contribute to substantially greater effective permeability compared to the matrix by orders of magnitude.

4.2 Practical Implications for Reservoir Management

The presence of permeability as the main influence on commercial potential can result from the strong influence of pore type and create several recommendations for practice. One important suggestion is that blanket cutoffs for porosity such as ignoring intervals with ϕ less than 10% creates misleading conclusions about commercial viability. For example, some fractured intervals in the dataset that had a ϕ as low 4.5 % still produced commercially because of the existence of fracture corridors (CP-0275). Additionally, several intervals in the same dataset have ϕ values greater than 15 percent, but are not commercially viable because of their microporous texture (CP-0090). Thus, we suggest the use of the T_2 NMR log cutoffs (after Coates et al. 1999) in order to distinguish microporosity from macroporosity, that is, T_2 values less than 33 ms from T_2 values greater than 33 ms. Completion decisions should reflect the preference for completing intervals of high macro-porosity or high fracture density irrespective of total porosity. In particular, we recommend perforating fractured or vuggy intervals

even when they have a ϕ value of less than 6 percent, and refraining from perforating tight microporous zones even when they have a ϕ value greater than 15 percent.

The specific permeability cutoffs (0.5 mD for vuggy intervals, 5 mD for interparticle-dominated rock, and fracture density >0.1 fractures/m) were derived from the simulation sensitivity analysis (Section 3.3, Table 9) and the multivariate regression coefficients (Table 10). A vuggy interval with permeability below 0.5 mD, even if porosity exceeds 15%, produced less than 100 STB/day in the base case model, failing to meet economic thresholds. For interparticle-dominated rock, the cutoff of 5 mD corresponds to the porosity–permeability power law where production becomes sensitive to drawdown. Fracture density of 0.1 fractures/m was identified as the threshold above which initial production exceeded 500 STB/day regardless of matrix porosity, based on field data from fractured wells (e.g., CP-0123 and CP-0305).

The recommendations presented herewere derived from the regression coefficients used for analysis and serve as a guide for improving well placement and reducing the incidence of uneconomic perforations.

4.3 Comparison with Previous Models

Our work builds upon, and extends, several established approaches. A detailed side-by-side comparison of previous studies versus the present work was already provided in **Table 1** (Section 1.5). Here, we briefly highlight the most salient improvements relative to five key contributions.

- **Lucia (1995, 2007):** While Lucia's petrophysical classification (interparticle, vuggy, fractured) is foundational, it remained descriptive and did not link pore types to production rate multiplie rs. Our study adds quantitative coefficients (0.39 for vug fraction, 0.52 for fracture density) that directly affect rate prediction.
- **Warren & Root (1963):** Their dual-porosity model assumes fractures as the sole high-permeability medium and fails in vuggy carbonates. Our findings demonstrate the need for a triple-porosity conceptual model (matrix – vugs – fractures), with vugs alone contributing 21 % of production rate variance.
- **Honarpour (2018):** The effect of relative permeability in mixed-wet carbonates is well recognized, but was not linked to pore geometry. We incorporate pore-type specific relative permeability curves derived from MICP and micro-CT data.
- **Okon et al. (2021):** Machine learning models (ANN, random forest) can achieve high permeability prediction accuracy, but they are black-box and lack physical basis, leading to poor extrapolation. Our physics-based regression (Kozeny–Carman exponent of 2.1 for interparticle pores) yields 12 % lower MAPE on blind wells.
- **Camacho-Velázquez et al. (2005):** Their triple-porosity pressure transient model is rigorous but requires numerical inversion and is not directly linked to routine production data. We provide a simple empirical equation (Eq. 2) that predicts initial production directly from core and log data with $R^2 = 0.81$.

Thus, rather than repeating the comprehensive tabular comparison found in Table 1, the above discussion focuses on how the present study advances each previous work. Readers seeking a full matrix of limitations, gaps, and contributions are referred to Table 1.

4.4 Limitations

Several limitations must be acknowledged when interpreting the results of this research. First, while the dataset included 500 carbonate samples from four regions (Middle East, North America, and Europe), it did not include all types of carbonates (e.g., chalk and dolomites), which have different diagenetic histories than those evaluated in this study (Ehrenberg & Nadeau, 2005). Therefore, care should be taken when attempting to extrapolate the data to pure chalk reservoirs (e.g., North Sea) or deep-seated dolomites. Second, we presented our production data as the initial rates based on fixed drawdown values and did not account for transient pressures or use decline curve analysis to forecast future production. Using well test analyses in conjunction with the current well tests may yield better estimates of permeability calculated from transient pressure readings rather than root-mean-square errors from core-derived measurements (Sharifi et al., 2023). Finally, since we did not consider geomechanically stress-related changes in permeability, our permeability estimates do not account for the effect of changing effective stress on production rates during depletion. Future efforts should include integration of the petrophysical models used in this study with coupled stress-flow simulations. Future studies can leverage open-access carbonate datasets (Scientific Data, 2023; 2024) to extend this analysis to additional lithologies and depositional environments. Nevertheless, because of the strong correlation established from blind test wells (R^2=0.81), we believe that our conclusions are sound for predicting production from all carbonates evaluated in this analysis.

Additionally, while the multivariate regression (Equation 2) was conducted using total vug fraction (Vvug) as a sole predictor variable, it does not differentiate between touching (connected) vugs versus separate (isolated) vugs. The micro-CT analysis

reported in Section 3.2 indicates that touching vugs can result in 1-2 orders of magnitude higher effective permeability compared to separate vugs with equivalent porosity and vug fraction. Since the current model does not take this distinction into account, results could lead to an under- or over-prediction of production from reservoirs containing a high inter-connectivity of vug networks relative to reservoirs having isolated vugs. Future work should incorporate a vug connectivity index (i.e., coordination number from micro-CT) into the regression framework.

5. Conclusion

There are many factors that affect how much oil can be produced from carbonate reservoirs, but this research shows that porosity alone is not a good predictor of production potential. With a correlation value of less than 0.2 globally for porosity, it does not explain all the variability in production rates. Permeability and the type of pores are better indicators of how quickly oil can be produced from carbonate reservoirs. Approximately 81% of the variance in initial production rates can be explained by the multivariate regression equation, $log\, Q = 0.87\, log\, k + 0.14\phi + 0.39 V_{\mathrm{vu}}{}^{g} + 0.52 F_{\mathrm{rac}} - 0.23$, which has been validated against blind well data and has much lower error (MAPE 18% vs. 42%) than current porosity/permeability transform methods. Fractures and vugs give initial production a boost but tend to deplete quickly; this will require future studies to confirm the long-term impact on production. For the purposes of reservoir simulation, effective permeability should be obtained from pore type logs instead of using generic $\phi - k$ transformations. Image logs and the NMR T_2 cutoff should also be used to map vug and fracture intensity, therefore optimally completing the well completion zone. The following cutoffs for determining economic production based on permeability were revised: >0.5 mD for vuggy intervals, >5 mD for interparticle-dominated rock, any fracture density greater than 0.1 fractures/meter may be economic regardless of the porosity in the matrix. Future research opportunities include expanding this analysis to include transient production data, such as pressure buildup analysis; incorporating stress-dependent permeability calculations to address reservoir depletion; and developing a carbonate-specific relative permeability correlation based on pore throat sorting. The proposed pore-type-based correction factor for Darcy's equation offers a practical, field-ready tool for improving production forecasts and completion strategies in heterogeneous carbonate reservoirs.

References

[1] Ahmadi, M. A., Ahmadi, M. R., Hosseini, S. M., & Ebadi, M. (2014). Connectionist model predicts the porosity and permeability of petroleum reservoirs by means of petro-physical logs: Application of artificial intelligence. *Journal of Petroleum Science and Engineering*, 123, 183-200.

[2] Barree, R. D., & Conway, M. W. (2004, September). Beyond beta factors: a complete model for Darcy, Forchheimer, and trans-Forchheimer flow in porous media. In *SPE Annual Technical Conference and Exhibition* (SPE-89325). SPE.

[3] Camacho-Velazquez, R., Vasquez-Cruz, M., Castrejon-Aivar, R., & Arana-Ortiz, V. (2005). Pressure-transient and decline-curve behavior in naturally fractured vuggy carbonate reservoirs. *SPE Reservoir Evaluation & Engineering*, 8(02), 95-112.

[4] Choquette, P. W., & Pray, L. C. (1970). Geologic nomenclature and classification of porosity in sedimentary carbonates. *AAPG Bulletin*, 54(2), 207-250.

[5] Coates, G. R., Xiao, L., & Prammer, M. G. (1999). NMR logging: Principles and applications, 85-87.

[6] Deutsch, C. V., & Journel, A. G. (1992). *Geostatistical software library and user's guide*. New York, 119(147), 578.

[7] Dong, H., & Blunt, M. J. (2009). Pore-network extraction from micro-computerized-tomography images. *Physical Review E*, 80(3), 036307.

[8] Ehrenberg, S. N., & Nadeau, P. H. (2005). Sandstone vs. carbonate petroleum reservoirs: A global perspective on porosity-depth and porosity-permeability relationships. *AAPG Bulletin*, 89(4), 435-445.

[9] Esrafili-Dizaji, B. (2026). Paleogeographic Controls on Porosity Evolution in Dolomitized vs. Karstified Reservoirs: Insights from the Zagros and Persian Gulf Carbonate Reservoirs. *Journal of the Geological Society*, jgs2025-167.

[10] Forchheimer, P. (1901). Wasserbewegung durch Boden. *Zeitschrift des Vereines Deutscher Ingenieure*, 45(50), 1781-1788.

[11] Honarpour, M. M. (2018). *Relative permeability of petroleum reservoirs*. CRC Press.

[12] Jennings, J. W., & Lucia, F. J. (2003). Predicting permeability from well logs in carbonates with a link to geology for interwell permeability mapping. *SPE Reservoir Evaluation & Engineering*, 6(04), 215-225.

[13] Klinkenberg, L. J. (1941). The permeability of porous media to liquids and gases. *Drilling and Production Practice*, 200-213.

[14] Lucia, F. J. (1995). Rock-fabric/petrophysical classification of carbonate pore space for reservoir characterization. *AAPG Bulletin*, 79(9), 1275-1300.

[15] Lucia, F. J. (2014). *Carbonate reservoir characterization: An integrated approach*. Springer Berlin.

[16] Nelson, P. H. (1994). Permeability-porosity relationships in sedimentary rocks. *The Log Analyst*, 35(03).

[17] Okon, A. N., Adewole, S. E., & Uguma, E. M. (2021). Artificial neural network model for reservoir petrophysical properties: porosity, permeability and water saturation prediction. *Modeling Earth Systems and Environment*, 7(4), 2373-2390.

[18] Pittman, E. D. (1992). Relationship of porosity and permeability to various parameters derived from mercury injection-capillary pressure curves for sandstone. *AAPG Bulletin*, 76(2), 191-198.

[19] Purcell, W. R. (1949). Capillary pressures – their measurement using mercury and the calculation of permeability therefrom. *Journal of Petroleum Technology*, 1(02), 39-48.

[20] *Scientific Data*. (2023). Full scale, microscopically resolved tomographies of sandstone and carbonate rocks augmented by experimental porosity and permeability values. *Scientific Data*, 10, 368. https://doi.org/10.1038/s41597-023-02259-z

[21] Sharifi, J., Moghaddas, N. H., Saberi, M. R., & Mondol, N. H. (2023). A novel approach for fracture porosity estimation of carbonate reservoirs. *Geophysical Prospecting*, 71(4), 664-681.

[22] Sulieman, H., Jouini, M. S., Alsuwaidi, M., Al-Shalabi, E. W., & Al Jallad, O. A. (2024). Multiscale investigation of pore structure heterogeneity in carbonate rocks using digital imaging and SCAL measurements: a case study from Upper Jurassic limestones, Abu Dhabi, UAE. *PLOS ONE*, 19(2), e0295192.
[23] Warren, J. E., & Root, P. J. (1963). The behavior of naturally fractured reservoirs. *Society of Petroleum Engineers Journal*, 3(03), 245-255.
[24] Xu, X., Wei, G. Q., & Yang, Z. M. (2013). The productivity calculation method of a carbonate reservoir. *Petroleum Science and Technology*, 31(3), 301-309.